

Error-feedback Stochastic Modeling Strategy for Time Series Forecasting with Convolutional Neural Networks

Xinze Zhang^{a,1}, Kun He^{b,1}, Yukun Bao^{a,*}

^aCenter for Modern Information Management, School of Management,
Huazhong University of Science and Technology, Wuhan, 430074 CN

^bSchool of Computer Science & Technology,
Huazhong University of Science and Technology, Wuhan, 430074 CN

Abstract

Despite the superiority of convolutional neural networks demonstrated in time series modeling and forecasting, it has not been fully explored on the design of the neural network architecture and the tuning of the hyper-parameters. Inspired by the incremental construction strategy for building a random multilayer perceptron, we propose a novel Error-feedback Stochastic Modeling (ESM) strategy to construct a random Convolutional Neural Network (ESM-CNN) for time series forecasting task, which builds the network architecture adaptively. The ESM strategy suggests that random filters and neurons of the error-feedback fully connected layer are incrementally added to steadily compensate the prediction error during the construction process, and then a filter selection strategy is introduced to enable ESM-CNN to extract the different size of temporal features, providing helpful information at each iterative process for the prediction. The performance of ESM-CNN is justified on its prediction accuracy of one-step-ahead and multi-step-ahead forecasting tasks respectively. Comprehensive experiments on both the synthetic and real-world datasets show that the proposed ESM-CNN not only outperforms the state-of-art random neural networks, but also exhibits stronger predictive power and less computing overhead in comparison to trained state-of-art deep neural network models.

Keywords: Convolutional neural network, error-feedback stochastic modeling, time series forecasting.

1. Introduction

Recent studies have revealed that convolutional neural network (CNN), which benefits from its strength in extracting local features via multiple convolutional filters and learning representation by fully connected layers, has been successfully implemented for time series forecasting that is of great importance in real world applications, such as finance [1, 2], energy [3, 4], and electric load [5, 6].

*Corresponding author

Email address: yukunbao@hust.edu.cn (Yukun Bao)

¹The first two authors contribute equally to this work.

The importance of time series forecasting and the applications of CNNs for modeling it have raised increasing attention to construct CNNs for time series prediction. As for the model selection, constructing a CNN commonly follows a typical paradigm, which is to determine and fix the hyper-parameters (i.e., neural architecture, learning rate, and training epochs) first, and then train the network based on some gradient descent optimization methods, making it inflexible and extremely laborious to evolve the hyper-parameters to build CNNs [7]. Hence, constructing a powerful CNN for time series prediction efficiently is focused in this study.

Researchers have investigated many methods on the model selection for building the forecasting model. Hu et al. [8] presented a hybrid PSO-SVR forecasting method, which used particle swarm optimization (PSO) to search optimal support vector regression (SVR) parameters. Flores et al. [9] evolved auto-regression moving average (ARMA) and multilayer perceptron (MLP) for time series forecasting by using genetic algorithm to indicate which variables are active in ARMA or to optimize the hidden neurons, activation functions and other configurations of MLP. Further, Elsken et al. [10] provided a survey on searching the hyper-parameters of neural network (NN) models, which concludes the common practice of evolving NN is to set up a search space of hyper-parameters defining the network architecture and then search the optimal parameters.

However, there exist imperfections in existing researches. For example, during the search phase of evolving CNN models, the candidate model configurations (e.g., the number of the filters, the type of activation functions and pooling layers, the size of convolutional and pooling filters) are fixed and then the weight parameters of the defined architectures are trained with a number of epochs, only after that, the candidate hyper-parameters can be evaluated. Unfortunately, it is extremely time-consuming of training many different model configurations [11].

In contrast, random CNN with untrained stochastic filters can be considered as an alternative option. It is suggested that stochastic filters that are iteratively generated to one convolutional layer after another can perform as well as trained filters for image representation inverting, texture synthesis, and style transfer [12]. The authors built a CNN architecture called VGG² with a stacked random strategy. For each layer they sampled several sets of weights in Gaussian distribution, selected one set of weights with the lowest inverting loss, and fixed the weights of each layer in forwarding order. Another try in audio identification showed that audio texture produced by trained one-dimensional CNN was found inferior to those produced by a random CNN [13]. Yu et al.[14] further showed that the precision of a CNN with random filters is close to a CNN of the same architecture but with trained filters in three scenarios of time series forecasting. Despite that random CNN is comparable to pre-trained CNN in some deep learning tasks, however, it is still hard to model the time series steadily due to the inner stochasticity.

In this study, we propose a novel error-feedback stochastic modeling based convolutional neural network (ESM-CNN) by incrementally generating new convolution filters and the corresponding fully connected layer's neuron to forecast the time series. Different from the existing method that updates all the output weights [15, 16], in order to avoid overfitting, we iteratively add neurons of the error-feedback fully connected layer to the filters and calculate the parameters. Furthermore, we propose a greedy based filter selection method to generate convolution filters with multiple filter sizes in constructing ESM-CNN, enabling ESM-CNN to extract different temporal patterns for the prediction.

The main contributions of this study are summarized as follows:

- We propose a novel error-feedback stochastic modeling strategy to efficiently craft a pow-

²https://www.robots.ox.ac.uk/vgg/research/very_deep/

erful CNN, called ESM-CNN, for time series forecasting task. An ESM-CNN is built by incrementally generating new random filters to promote its construction efficiency, and individually configuring the corresponding neurons of the error-feedback fully connected layer to theoretically guarantee its forecasting performance as well as improving its stability.

- A greedy based filter selection method is introduced to select the convolution filters from the randomly generated candidates with different filter sizes, enabling ESM-CNN to extract different temporal patterns and select the convolution filters adaptively.
- Comprehensive experiments on simulated and real-world datasets demonstrate the efficiency and the effectiveness of the proposed ESC strategy as well as filter selection method of ESM-CNN for time series prediction. ESM-CNN exhibits strong predictive power, with low computation overhead and good generalization ability compared with standard random neural networks and deep neural networks.

The rest of the paper is organized as follows. Section 2 introduces related works on CNN and random MLP, indicating the motivation of our work. Details about the proposed ESM-CNN modeling strategy are depicted in Section 3. Section 4 presents details on dataset description, counterparts selection, accuracy measure, and experimental procedure. Experimental results are presented and discussed in Section 5. Finally, Section 6 concludes this work.

2. Related works

To clearly illustrate the motivation of the proposed error-feedback stochastic modeling strategy of constructing a CNN for time series prediction, the preliminary formulation and related works of implementing CNN as well as random MLP for time series forecasting are introduced briefly.

2.1. Forecasting formulation

The essence of time series forecasting is a type of function approximation procedure. As defined in [17], an univariate time series prediction problem refers to forecasting future values of a time series based on its past values. That is, given a time series with T observations $\{x_1, \dots, x_T\}$ and the next H -steps-ahead observations $\{x_{T+1}, \dots, x_{T+H}\}$, the univariate time series prediction problem can be formulated as learning a approximation function:

$$f : f(x_1, \dots, x_T) + e = \{x_{T+1}, \dots, x_{T+H}\} \quad (1)$$

to minimize the prediction error $\|e\|$. Here, f is the function approximated by the model constructed for the time series forecasting with the variable x . The model forecasts the future values from $T + 1$ to $T + H$, where H is the forecasting horizon. In the following, we give the formulation of implementing CNN and random MLP for time series forecasting.

2.2. Convolutional Neural Network

Convolutional neural network is developed by connecting filters to local fields on the input to perceptron [18]. With local connections, filters can extract elementary features that are likely to be useful across the entire time series. The outputs of such a set of filters constitute the feature maps [19]. And then, these feature maps are combined in higher layers, i.e., fully connected layers, to learn abstract representations. Here we briefly introduce a typical convolutional neural network for time series forecasting, which consists of a single convolutional layer to extract feature maps, a single pooling layer to subsample the feature maps, and a fully connected layer to learn the outputs.

Consider that a time series data $D = \{(X_i, Y_i) \in (\mathbb{R}^T \times \mathbb{R}^H)\}_{i=1}^N$ is composed of N samples with T observations $X_i = [x_1, \dots, x_T]^T$ for forecasting the next H -steps-ahead observations $Y_i = [x_{T+1}, \dots, x_{T+H}]^T$. The CNN with C convolution filters can be expressed as:

$$f_C = \sum_{j=1}^C \left(\sum_{i=1}^{T-K+2} \beta_j^i p_j^i \right) + \beta_0, \quad (2)$$

$$p_j^i = \frac{\sum_{k_p=1}^{K_p} m_j^{i+k_p-1}}{K_p}, \quad i = 1, \dots, T - K_p - K_m + 2, \quad (3)$$

$$m_j^t = \sigma \left(\sum_{k_m=1}^{K_m} w_j^{k_m} x_{t+k_m-1} + b_j \right), \quad t = 1, \dots, T - K_m + 1, \quad (4)$$

where $K = K_p + K_m$, K_p and K_m are the kernel size of the pooling and convolution operation, respectively. p_j denotes the feature map vector $[p_j^1, \dots, p_j^{T-K+2}]^T$ sequentially down-sampled from m_j by the average pooling, m_j denotes the feature map vector $[m_j^1, \dots, m_j^{T-K_m+1}]^T$ sequentially extracted by the j -th filter with K_m size of local connections from the input time series. And $\sigma(\cdot)$ is a nonlinear activation function, set as sigmoid in this work, $w_j = [w_j^1, \dots, w_j^{K_m}]$ and b_j are the weight and bias of the j -th filter.

CNN usually uses the pooling operation to subsample the feature maps. The advantage of this operation is to reduce the convolutional output band, and be more robust to variations in feature maps [20]. Average or maximum pooling is commonly utilized for time series analysis [21–23], and average pooling is selected in this study. Besides, $[\beta_1^1, \beta_1^2, \dots, \beta_C^{T-K+2}]$ ($\beta_j^i = [\beta_j^{i,1}, \dots, \beta_j^{i,H}]^T$) and β_0 are respectively the weights and bias in the fully connected layer that are linked to all feature map vectors.

Since all the weights and biases are gradient-based trained with back-propagation, CNN can extract features via filters from the input time series and linearly link these features to predictions by the fully connected layer. However, the fixed architecture of trained CNN requires predefined hyper-parameters, which is computationally expensive to tune the number of filters, training epochs, and other configurations.

2.3. Random Multilayer Perceptron

Random multilayer perceptron, which is initially proposed by [24] and further developed on the random vector version of the functional-link (RVFL) network [15] as well as extreme learning machine (ELM) network [25], uses the randomly initialized and fixed hidden layers and analytically computed output layer to build a MLP. The structures of these three typical random MLPs are shown in Figure 1.

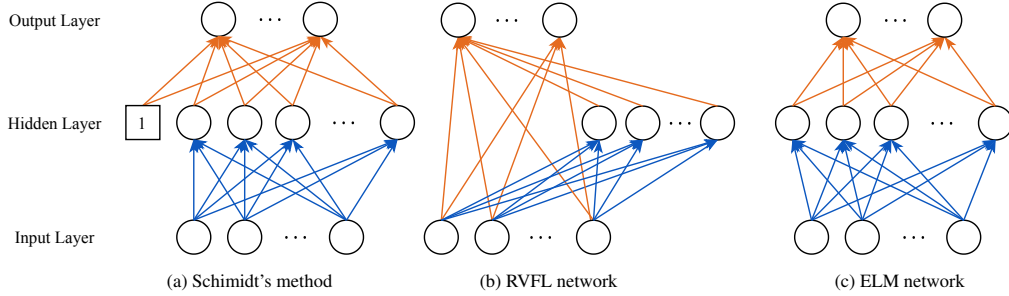


Figure 1: Typical random multilayer perceptron, where the blue arrows denote the randomly initialized and fixed hidden weights, and the yellow arrows represent the analytically determined output weights.

Inspired by the pioneering work [15, 24, 25], many researches have been conducted for developing random MLPs. Pao et al. [26] indicated that a single step pseudo-inverse solution was sufficed for RVFL. Scardapane et al. [27] proposed the distributed learning algorithms for RVFL by leveraging the subsets of the data to train the local models and find the common output weights of the master model. Zhang et al. [28] used a sparse and regular autoencoder to make an unsupervised learning RVFL network. Huang et al. [29] investigated the relationship between ELM and support vector machine and extend ELM with kernel methods. Kasun et al. [30] introduced orthogonal random feature mapping to build a ELM-based autoencoder, providing a promising solution to representation learning.

Since the conventional random MLPs are proposed and constructed in the deterministic method, it is also quite challenging to select the proper parameters, such as the number of the hidden units, for the practical implementations. To resolve this issue, an incrementally constructive method has been leveraged to build random MLPs. Huang et al. [31] proposed an incremental ELM (IELM) by iteratively adding the randomly generated neural unit to the hidden layer of the network and proved it can converge to any continuous target function. Wang and Li [16] developed an incremental random MLP with stochastic configuration algorithms and named the model as stochastic configuration network (SCN), where the hidden layer was built incrementally with selected random neurons and the output layer was determined via the least squares method.

The implementation of incremental random MLP for time series modeling and forecasting is described below. Assume a random MLP has generated L hidden neurons in its single fully connected hidden layer:

$$f_L = \sum_{j=1}^L \beta_j g_j \left(\sum_{i=1}^T w_j^i x_i + b_j \right), \quad (5)$$

where $w_j = [w_j^1, \dots, w_j^T]$ and b_j are respectively the weight and bias of the j -th neuron, $g(\cdot)$ is the sigmoid activation function. And the neurons are represented as $[g_1, \dots, g_L]^T$ with the corresponding output weights $[\beta_1, \dots, \beta_L]$, $\beta_j = [\beta_j^1, \dots, \beta_j^H]^T$, H is the prediction horizons. The prediction error is denoted as:

$$e_L = Y - f_L = [e_L^1, \dots, e_L^H]^T. \quad (6)$$

If $\|e_L\|$ is higher than a tolerance level ϵ , the random MLP incrementally adds a new random neuron g_{L+1} (w_{L+1} and b_{L+1}) to the hidden layer and updates the parameters of the output layer, where IELM directly generates a random hidden neuron and computes its corresponding output

weight. In contrast to IELM, SCN generates a new selected random hidden neuron that satisfies a supervisory condition and updates the whole parameters of the output layer.

So far, tremendous efforts have been devoted to develop theories and applications for random MLPs, and yield considerable performance for the regressions and predictions [16, 29, 31–34]. However, there are few works related to random CNN in the literature of time series forecasting. In this study, to craft a powerful CNN for time series prediction efficiently, an error-feedback stochastic modeling strategy is proposed and justified within CNN.

3. The ESM-CNN modeling strategy

To address the limitation of implementing CNN for time series forecasting, we propose an error-feedback stochastic modeling strategy of building a random convolutional neural network, called ESM-CNN, for time series forecasting. This section presents the implementation details and convergence analysis of ESM-CNN.

3.1. Error-feedback Stochastic Strategy

In order to efficiently construct a powerful CNN forecasting model, which benefits from the efficiency of random NNs and also tackles the instability of its inner randomness, we propose an error-feedback stochastic modeling strategy for constructing a random CNN. An ESM-CNN is built by incrementally generating new random filters to promote its efficiency, and individually configuring the corresponding neurons of the error-feedback fully connected layer to guarantee its forecasting performance with theoretical convergence property.

Specifically, assume that an ESM-CNN with C filters has been constructed within a single convolutional layer, which can be expressed as:

$$f_C = \sum_{j=1}^C \left(\sum_{i=1}^{T-K+2} \beta_j^i p_j^i + \beta_j^0 \right), \quad (7)$$

and briefly written as $f_C = \sum_{j=1}^C \sum_{i=0}^{T-K+2} \beta_j^i p_j^i$, where $\beta_j = [\beta_j^0, \beta_j^1, \dots, \beta_j^{T-K+2}]$ present the weight parameter and bias parameter of the fully connected layer linked with the j th subsampled filter, $p_j^0 = I$. Let the prediction error of ESM-CNN be denoted as

$$e_C = Y - f_C = [e_C^1, \dots, e_C^H]. \quad (8)$$

If the mean square error has not reached the tolerance level ϵ , ESM will generate a stochastic filter m_{C+1} with the corresponding pooling values p_{C+1} and fully connected layer neurons to CNN, where the parameters of the newly added fully connected layer neurons are individually calculated under the error-feedback from e_C via the least squares method:

$$[\beta_{C+1}^0, \dots, \beta_{C+1}^{T-K+2}] = \underset{\beta}{\operatorname{argmin}} \|e_C - \sum_{i=0}^{T-K+2} \beta_{C+1}^i p_{C+1}^i\|. \quad (9)$$

Through this strategy, it is guaranteed that the prediction error of the CNN is monotonically decreasing and converged, which is proved as follows. And the detailed manipulations for the derived formulas are provided in Appendix A.

Proof. The intermediate prediction error sequence $\tilde{e}_{C+1}^0, \dots, \tilde{e}_{C+1}^{T-K+2}$ and the intermediate parameters $\tilde{\beta}_{C+1}^0, \dots, \tilde{\beta}_{C+1}^{T-K+2}$ of the new added fully connected layer are introduced as:

$$\tilde{e}_{C+1}^{i+1} = \tilde{e}_{C+1}^i - \tilde{\beta}_{C+1}^{i+1} p_{C+1}^{i+1}, \quad i = 0, \dots, T - K + 1,$$

where

$$\begin{aligned} \tilde{\beta}_{C+1}^{i+1} &= [\tilde{\beta}_{C+1}^{i+1,1}, \dots, \tilde{\beta}_{C+1}^{i+1,h}, \dots, \tilde{\beta}_{C+1}^{i+1,H}], \\ \tilde{\beta}_{C+1}^{i+1,h} &= \langle \tilde{e}_{C+1}^{i,h}, p_{C+1}^{i+1} \rangle / \|p_{C+1}^{i+1}\|^2, \quad h = 1, \dots, H, \end{aligned}$$

and

$$\begin{aligned} \tilde{e}_{C+1}^0 &= e_C - \tilde{\beta}_{C+1}^0 p_{C+1}^0, \\ \tilde{\beta}_{C+1}^0 &= [\tilde{\beta}_{C+1}^{0,1}, \dots, \tilde{\beta}_{C+1}^{0,h}, \dots, \tilde{\beta}_{C+1}^{0,H}], \\ \tilde{\beta}_{C+1}^{0,h} &= \langle e_C^h, p_{C+1}^0 \rangle / \|p_{C+1}^0\|^2, \quad h = 1, \dots, H, \end{aligned}$$

making

$$\tilde{e}_{C+1}^{T-K+2} = e_C - \sum_{i=0}^{T-K+2} \tilde{\beta}_{C+1}^i p_{C+1}^i.$$

Since the parameters of the new added error-feedback fully connected layer are calculated by the least square method:

$$[\beta_{C+1}^0, \dots, \beta_{C+1}^{T-K+2}] = \underset{\beta}{\operatorname{argmin}} \|e_C - \sum_{i=0}^{T-K+2} \beta_{C+1}^i p_{C+1}^i\|,$$

the basic inequality between $\|e_{C+1}\|^2$ and $\|\tilde{e}_{C+1}^{T-K+2}\|^2$ holds:

$$\|e_{C+1}\|^2 = \min_{\beta} \|e_C - \sum_{i=0}^{T-K+2} \beta_{C+1}^i p_{C+1}^i\|^2 \leq \|e_C - \sum_{i=0}^{T-K+2} \tilde{\beta}_{C+1}^i p_{C+1}^i\|^2 = \|\tilde{e}_{C+1}^{T-K+2}\|^2.$$

Besides, the intermediate prediction error sequence is monotonically decreasing as:

$$\begin{aligned} & \|\tilde{e}_{C+1}^{i+1}\|^2 - \|\tilde{e}_{C+1}^i\|^2 \\ &= \sum_{h=1}^H \left(\langle \tilde{e}_{C+1}^{i,h} - \tilde{\beta}_{C+1}^{i+1,h} p_{C+1}^{i+1}, \tilde{e}_{C+1}^{i,h} - \tilde{\beta}_{C+1}^{i+1,h} p_{C+1}^{i+1} \rangle - \langle \tilde{e}_{C+1}^{i,h}, \tilde{e}_{C+1}^{i,h} \rangle \right) \\ &= \sum_{h=1}^H \left(\langle \tilde{\beta}_{C+1}^{i+1} p_{C+1}^{i+1}, \tilde{\beta}_{C+1}^{i+1} p_{C+1}^{i+1} \rangle - 2 \langle \tilde{e}_{C+1}^{i,h}, \tilde{\beta}_{C+1}^{i+1} p_{C+1}^{i+1} \rangle \right) \\ &= \sum_{h=1}^H \left(- \langle \tilde{e}_{C+1}^{i,h}, p_{C+1}^{i+1} \rangle^2 / \|p_{C+1}^{i+1}\|^2 \right) \\ &\leq 0. \end{aligned}$$

And the inequality between $\|\tilde{e}_{C+1}^0\|^2$ and $\|e_C\|^2$ can be proven by:

$$\begin{aligned}
& \|\tilde{e}_{C+1}^0\|^2 - \|e_C\|^2 \\
&= \sum_{h=1}^H \left(\langle e_C^h - \tilde{\beta}_{C+1}^{0,h} p_{C+1}^0, e_C^h - \tilde{\beta}_{C+1}^{0,h} p_{C+1}^0 \rangle - \langle e_C^h, e_C^h \rangle \right) \\
&= \sum_{h=1}^H \left(\langle \tilde{\beta}_{C+1}^{0,h} p_{C+1}^0, \tilde{\beta}_{C+1}^{0,h} p_{C+1}^0 \rangle - 2 \langle e_C^h, \tilde{\beta}_{C+1}^{0,h} p_{C+1}^0 \rangle \right) \\
&= \sum_{h=1}^H \left(- \langle e_C^h, p_{C+1}^0 \rangle^2 / \|p_{C+1}^0\|^2 \right) \\
&\leq 0.
\end{aligned}$$

Then, the convergence of ESM-CNN can be guaranteed by:

$$\|e_{C+1}\|^2 \leq \|\tilde{e}_{C+1}^{T-K+2}\|^2 \leq \|\tilde{e}_{C+1}^0\|^2 \leq \|e_C\|^2.$$

□

There are three major benefits from conducting the error-feedback calculation individually, rather than globally updating all parameters of the fully connected layer. The overhead calculation of updating all weights and biases of fully connected layer is more expensive, especially in the situation that a number of filters have been generated. Besides, as the random CNN successively adds the filters, a progressively increasing number of features are involved in the construction process, making the least squares method encounter the ill-posed problem and lose accuracy [35]. Furthermore, the error-feedback fully connected layers use the information of prediction error in the last construction process, which is indeed to steadily compensate the prediction error at each process and reduces the uncertainty caused by randomness.

3.2. Filter Selection Strategy

As per the convolution filter selection problem, we propose a greedy based method to select the random filters with multiple sizes in the construction process of ESM-CNN, such that the different temporal patterns can be extracted.

Assume an ESM-CNN with single convolutional layer has been constructed with C filters, as expressed in Equation 7. Then, following the uniform distribution $[-\lambda, \lambda]$, a batch of subsampled filter candidates are randomly generated $\{p_{C+1,s}\}_{s=1}^S$ with the corresponding convolutional and pooling filter sizes $\{(K_{m,s}, K_{p,s})\}_{s=1}^S$. To evaluate the filter candidates, the filter score $\Delta_{C+1,s}$ which represents the prediction promotion after adding the filter candidate $p_{C+1,s}$ is proposed and calculated by:

$$\begin{aligned}
\Delta_{C+1,s} &= \|e_{C+1,s}\|^2 - \|e_C\|^2 \\
&= \|e_C - \sum_{i=0}^{T-K'+2} \beta_{C+1,s}^i p_{C+1,s}^i\|^2 - \|e_C\|^2
\end{aligned} \tag{10}$$

where $K' = K_{m,s} + K_{p,s}$, $p_{C+1,s}$ is computed as Equation 3, and $\beta_{C+1,s}$ is solved as Equation 9.

Based on the filter score, the best subsampled filter p_{C+1}^* that achieves the maximum promotion is selected from the filter candidates, which is:

$$p_{C+1}^* = \underset{p_{C+1,s}}{\operatorname{argmax}} \{ \Delta_{C+1,s}, s = 1, \dots, S \}. \quad (11)$$

After that, the parameters of the corresponding error-feedback fully connected layer are calculated by Equation 9. Through this filter selection strategy, a variety of temporal patterns are step-wisely extracted for ESM-CNN.

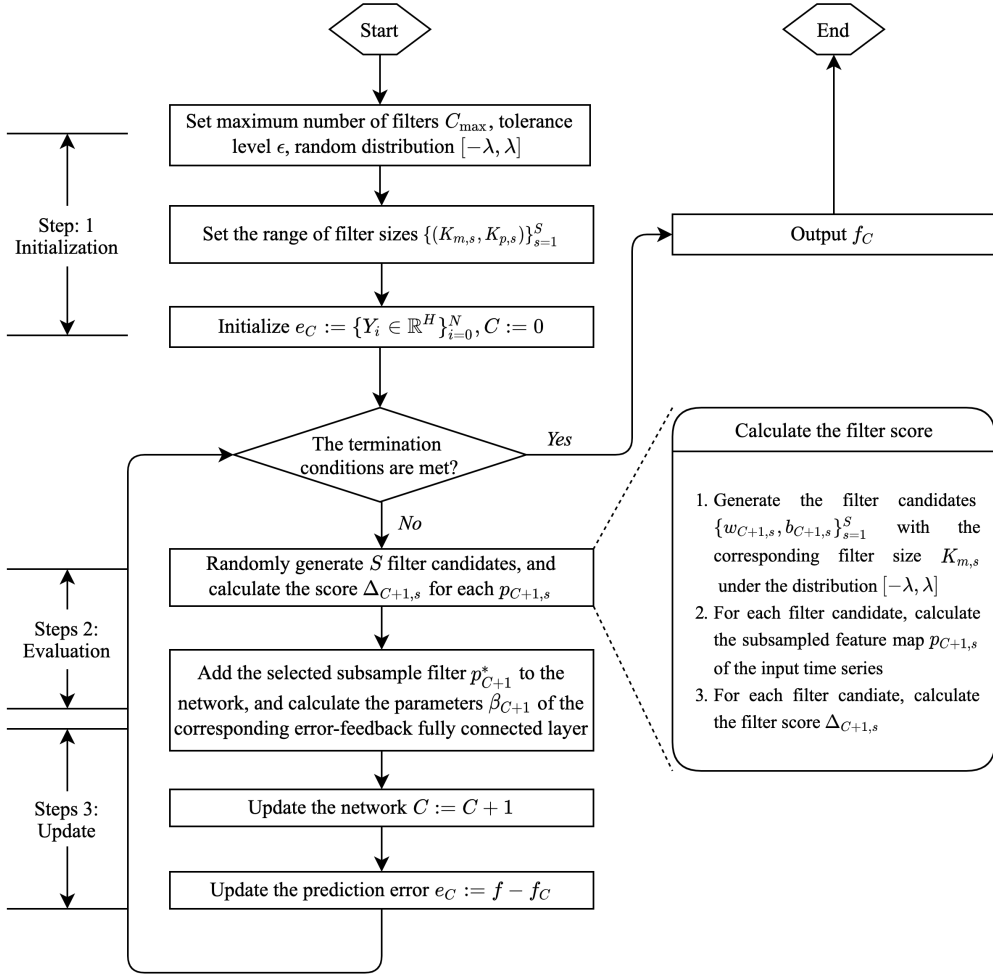


Figure 2: Flowchart of the proposed ESM-CNN modeling strategy.

3.3. Implementation of ESM-CNN

This subsection details the implementation of the proposed ESM-CNN strategy, as illustrated in Algorithm 1 and Figure 2. Considering the filter selections, the major operations of ESM-CNN

modeling strategy consist of the initialization, evaluation, updating, and a preprocessing of normalization. For data preprocessing, the data sets are first scaled to standard normal distribution.

- 1) **Initialization.** Consider that a time series data $D = \{(X_i, Y_i) \in (\mathbb{R}^T \times \mathbb{R}^H)\}_{i=1}^N$ is composed of N samples with T observations $[x_1, \dots, x_T]^T$ for forecasting the next H -steps-ahead observations $[x_{T+1}, \dots, x_{T+H}]^T$. The proposed ESM-CNN is initialized with several basic configurations, including the initial prediction error e_0 that is defined as the forecasting target $e_0 = [x_{T+1}, \dots, x_{T+H}]^T$, the maximum number of filters C_{\max} , the expected tolerance ϵ , the random distribution $[-\lambda, \lambda]$, and the candidate convolution filter sizes as well as the candidate pooling filter sizes $\{(K_{m,s}, K_{p,s})\}_{s=1}^S$. Concerning the selection of those configurations, it is yet a challenging model selection problem. In this work, the expected tolerance ϵ is set as 0 to further explore the forecasting performance of the proposed ESM-CNN, the maximum number of filters C_{\max} is set as 100 to ensure the convergence of the modeling. Besides, the distribution $[-\lambda, \lambda]$ is set as $[-0.5, 0.5]$ and the candidate convolution filter sizes are set as $\{K_{m,s}\}_{s=1}^S = \{T/3, T/4, T/5, T/6\}$ through our experimental experience. Following the analysis in [20], the average pooling with $K_p = 3$ is adopted in the experiments.
- 2) **Evaluation.** After the initialization, the proposed ESM-CNN steps into the constructing process with no initialized filter in the convolutional layer as $C := 0$. To select the convolutional filters in the constructing process, a greedy based filter selection strategy is proposed to evaluate and select the random filters with different filter sizes. In each iteration C , we first build a filter candidate set wherein the candidate filters are randomly generated following the distribution $[-\lambda, \lambda]$. For each candidate filter, we construct a candidate architecture by adding it to the network, then calculate its subsampled feature maps $\{p_{C+1,s}\}_{s=1}^S$ and obtain the corresponding score $\{\Delta_{C+1,s}\}_{s=1}^S$ by Equation 10. After that, we evaluate the candidate filters and select the best one which yields the most significant prediction promotion.
- 3) **Update.** Following the evaluation, we calculate the parameters of the error-feedback fully connected layer that is linked with the selected filter by Equation 9. Then, the selected convolution filter and the corresponding error-feedback fully connected layer are configured into the network, widening the convolutional layer as $C := C + 1$. Meanwhile, the prediction error is steadily decreasing and updated as $e_C := f - f_C$. Once the termination conditions are satisfied, a powerful CNN is efficiently crafted for time series forecasting.

4. Experimental Design

4.1. Dataset Description

To evaluate the performance of the proposed ESM-CNN modeling strategy and the counterparts in terms of forecasting accuracy, one synthetic time series dataset, i.e., *first order autoregression* (AR1), as well as two real-world dataset, i.e., *bitcoin price* (BTC) and *influenza-like illness* (ILI), are used for experiments.

The *first order autoregression* time series are recognized as benchmark time series that have been commonly used and reported by a number of studies related to time series modeling and forecasting [36, 37]. As an example of stochastic trend series that exhibits complex and chaotic behavior, AR1 is synthesized in Equation 12:

$$x_t = \alpha + x_{t-1} + \varepsilon_t, \quad (12)$$

Algorithm 1 ESM-CNN Modeling Algorithm

Input: time series dataset D ,

- maximum number of convolution filters C_{\max} ,
- tolerance level ϵ ,
- random distribution $[-\lambda, \lambda]$,
- convolution and pooling filter sizes $\{(K_{m,s}, K_{p,s})\}_{s=1}^S$.

Output: subsampled convolution filters $\{p_c\}_{c=1}^C$,
corresponding error-feedback fully connected layers $\{\beta_c\}_{c=1}^C$, where the weight is $[\beta_c^1, \dots, \beta_c^{T-K+2}]$ and the bias is β_c^0 .

- 1: Initialize $e_0 := \{Y_i \in \mathbb{R}^H\}_{i=1}^N$, $C := 0$.
 - 2: **while** $C + 1 \leq C_{\max}$ and $\|e_C\|_F \geq \epsilon$ **do**
 - 3: Randomly generate S 1D filter candidates following the distribution $[-\lambda, \lambda]$ and the corresponding convolution as well as the pooling filter size $(K_{m,s}, K_{p,s})$.
 - 4: Calculate the subsampled feature maps $\{p_{C+1,s}\}_{s=1}^S$ and the corresponding scores $\{\Delta_{C+1,s}\}_{s=1}^S$.
 - 5: $p_{C+1}^* = \operatorname{argmax}\{\Delta_{C+1,1}, \dots, \Delta_{C+1,S}\}$ is selected and added to f_C .
 - 6: Calculate the parameters of the error-feedback fully connected layer linked with the newly added filter $[\beta_{C+1}^0, \dots, \beta_{C+1}^{T-K+2}]$.
 - 7: Update the number of filters $C := C + 1$.
 - 8: Update the current prediction error $e_C := f - f_C$.
 - 9: **end while**
 - 10: **return:** Subsampled convolution filters $\{p_1, \dots, p_C\}$, and parameters of the corresponding error-feedback fully connected layer $\{\beta_1, \dots, \beta_C\}$.
-

where $\alpha = 0.01$, $\varepsilon_t \sim i.i.d. U(-0.25, 0.25)$, and 500 observed values are simulated.

The *bitcoin price* constitutes a significant part of the economics and block chain markets. Through bitcoin price forecasting, the investors can be supported for making proper decisions. However, the bitcoin price behaves hardly-predictable fluctuations, making accurate prediction of bitcoin price forecasting be an important and challenging task. In this real-world forecasting task, we concern two-hourly bitcoin to U.S. dollar close price, and 2181 observed values from May 2020 to March 2021 are drawn from the tradeview service.³

The *influenza-like illness* not only keeps seriously threatening public health but also makes it more challenging for defending against coronaries disease 2019 (COVID-19) since the ILI shares widely common symptoms with COVID-19. Thus, it is crucial to provide accurate influenza prediction to support the public health administrations, making ILI prediction be selected in this study. In this case, the ILI data is extracted from the Chinese National Influenza Center's website,⁴ and consists of 533 weekly ILI percentage values in southern China from January 2010 to March 2020.

Both three datasets are used for evaluating the performance of the proposed ESM-CNN modeling strategy and the counterparts. Each time series is split into three parts for training, validation and testing following the common relation of 0.64, 0.16 and 0.2. The embedding dimension T of AR1, BTC, and ILI are 15, 24 (two days), and 26 (half year) respectively.

³<https://www.tradingview.com/symbols/BTCUSD/>

⁴<http://www.chinaivdc.cn/cnic/zyzx/lgzbb/>

Table 1: The summary information of the forecasting tasks.

Dataset	AR1	BTC	ILI
Observed values	500	2181	533
Embedding dimension	15	24	26
Prediction horizons	1, 3, 6	1, 3, 6	1, 4, 8

We examine one-step-ahead and multi-step-ahead predictions to justify the performance of the proposed modeling strategies over different horizons. For multi-step-ahead forecasting, the multiple-input multiple-outputs strategy [38], often advocated in standard time series textbooks and reviews, is implemented. As shown in Table 1, the multi-step-ahead horizons for the AR1 dataset are set as 3 and 6. The forecasting horizons for BTC dataset are selected as six hours and half day (3 two-hours and 6 two-hours). The prediction horizons for ILI dataset are set as about one month and two months (4 weeks and 8 weeks).

4.2. Counterparts Selection

4.2.1. RVFL, IELM and SCN

To compare the stochastic filters with random hidden neurons, RVFL[15], IELM[31] and SCN[16] are selected as counterparts. The parameters of RVFL, IELM and SCN (i.e., distributions of randomly generating neurons, tolerance level) are kept consistent with ESM-CNN to control the impact variables in the comparisons. And the pre-defined number of hidden neurons in RVFL is kept same with the maximum number of hidden neurons and filters in IELM, SCN and ESM-CNN.

4.2.2. GS-CNN, DeepAR and CLSTM

Besides above mentioned random MLPs, CNN, recurrent neural network (RNN), and convolutional recurrent neural network (CRNN) are also selected as strong competitors. We implement a single convolutional layer CNN by using grid-search approach to select the network architecture, and name it as GS-CNN. We implement the RNN with DeepAR [39] which is built based on an autoregression long short term memory network (LSTM) and shows state-of-the-art performance on many forecasting tasks. Besides GS-CNN and DeepAR, we implement a convolutional long short term memory network [40] which couples the CNN and LSTM as CRNN, and denote this model as CLSTM. The hyper-parameters (i.e., optimization method, learning rate, and training epochs) of GS-CNN, DeepAR, and CLSTM are set and fine-tuned following trial and error fashion.

4.2.3. ES-CNN and Stoc-CNN

Furthermore, we perform an ablation study to verify the necessity of filter selection strategy and error-feedback mechanism in ESM-CNN. We remove the filter selection strategy and maintain the error-feedback in ESM-CNN, making an ablative counterpart as error-feedback stochastic convolutional neural network (ES-CNN). Furthermore, we remove the both error-feedback and filter selection strategies of ESM-CNN, making another ablative counterpart as vanilla stochastic convolutional neural network (Stoc-CNN)[14].

As for controlling variables in ablation experiments, the parameters of Stoc-CNN (i.e., distribution of randomly generating filters, number of filters) follow the same settings of ESM-CNN. And the maximum number of filters in ESM-CNN and ES-CNN are also kept consistent.

The codes and experimental logs are published in Github repository,⁵ including all details of the models used in this study. Through these counterparts, we can explore and justify the effectiveness of ESM-CNN, which is the highlight of our work.

4.3. Accuracy Measure

To evaluate the forecasting accuracy of the proposed ESM-CNN modeling strategy and the selected counterparts from various aspects (i.e., percentage error and numerical error), three widely used statistic measures are selected, including mean absolute percentage error (MAPE), symmetric mean absolute percentage error (SMAPE), and root mean square error (RMSE) [41–43].

$$MAPE = \frac{1}{N} \sum_{i=1}^N \left| \frac{y_i - \hat{y}_i}{y_i} \right|. \quad (13)$$

$$SMAPE = \frac{1}{N} \sum_{i=1}^N \left| \frac{y_i - \hat{y}_i}{y_i + \hat{y}_i} \right|. \quad (14)$$

$$RMSE = \sqrt{\frac{1}{N} \sum_{i=1}^N (y_i - \hat{y}_i)^2}. \quad (15)$$

Here y_i and \hat{y}_i stand for the real value and the predicted value respectively.

4.4. Experimental Procedure

For the selected time series datasets, each of the datasets is first scaled with z-score method to map onto standard normal distribution,⁶ and split into a training, a validation set, and a testing set. The proposed ESM-CNN modeling strategy and the counterparts are fitted as well as cross-validated with the training set and the validation set. For preprocessed data, we convert the outputs back to their original scales. Then, the models can be estimated and directly compared for each forecasting horizons with the MAPE, SMAPE, and RMSE measures over all datasets.

Finally, we execute each model 20 times using CUDA 10.1 accelerated Pytorch framework⁷ on a Ubuntu 20.04 server with Intel 8700K CPU and Nvidia GTX 1070 GPU, and the averaged performance is reported in the next section. Furthermore, upon the requests from reviewers, eight more real-world datasets and three more linear competing models were selected to extend the present experiment, and the results are provided in Appendix B.

5. Results and discussions

5.1. Comparison on Prediction Accuracy

The prediction performance of the proposed ESM-CNN, the state-of-art training base counterparts (GS-CNN, DeepAR and CLSTM) and random based counterparts (RVFL, IELM and SCN) as well as ablative counterparts (Stoc-CNN and ES-CNN) on all datasets are respectively shown in Table 2, Table 3, and Table 4, examined in terms of three accuracy measures (MAPE, SMPAE, and RMSE). From the third column to the last column, the mean measure values and the standard deviation (in the bracket) are listed. For each row of the statistics, the entry with the smallest value is in boldface and marked with an asterisk, and the second smallest value is set in boldface type.

Table 2: The average MAPE of ESM-CNN and the counterparts.

Dataset	H	Training			Random			Ablation		Ours
		GS-CNN	DeepAR	CLSTM	RVFL	IELM	SCN	Stoc-CNN	ES-CNN	ESM-CNN
ARI	1	1.06e-01	1.08e-01	8.88e-02	7.61e-01	9.84e-02	6.50e-02	6.10e+01	4.53e-02	3.49e-02*
		(7.38e-03)	(2.26e-02)	(1.42e-02)	(4.74e-01)	(1.47e-02)	(2.41e-02)	(2.52e+01)	(5.81e-03)	(5.01e-04)
	3	1.23e-01	1.64e-01	1.20e-01	1.17e+00	1.07e-01	9.53e-02	6.34e+01	6.41e-02	5.28e-02*
		(7.15e-03)	(3.46e-02)	(1.34e-02)	(5.85e-01)	(1.22e-02)	(1.97e-02)	(2.13e+01)	(5.21e-03)	(1.77e-03)
	6	1.48e-01	2.17e-01	1.24e-01	1.23e+00	1.26e-01	1.16e-01	1.54e+02	8.92e-02	7.70e-02*
		(6.41e-03)	(3.72e-02)	(1.84e-02)	(7.78e-01)	(1.74e-02)	(2.63e-02)	(8.02e+01)	(5.23e-03)	(2.32e-03)
BTC	1	6.27e-02	2.26e-01	4.09e-01	1.20e+00	1.85e-01	1.11e-01	2.14e+02	4.62e-02	2.70e-02*
		(6.37e-03)	(3.09e-02)	(2.34e-02)	(7.24e-01)	(2.98e-02)	(2.45e-02)	(1.90e+02)	(1.82e-02)	(4.98e-04)
	3	6.43e-02	1.98e-01	4.41e-01	1.13e+00	1.84e-01	1.29e-01	2.86e+02	4.73e-02	2.96e-02*
		(6.63e-03)	(3.80e-02)	(2.44e-02)	(4.82e-01)	(2.94e-02)	(2.62e-02)	(2.33e+02)	(1.76e-02)	(3.67e-04)
	6	6.49e-02	2.35e-01	4.61e-01	1.38e+00	1.84e-01	1.40e-01	3.32e+02	4.84e-02	3.26e-02*
		(6.28e-03)	(4.20e-02)	(9.60e-03)	(6.57e-01)	(3.06e-02)	(2.54e-02)	(3.00e+02)	(1.68e-02)	(2.65e-04)
ILI	1	1.28e-01	1.14e-01	9.50e-02	3.03e-01	1.38e-01	1.15e-01	2.48e+00	1.00e-01	8.93e-02*
		(2.30e-03)	(8.92e-03)	(2.64e-03)	(5.17e-02)	(8.14e-03)	(9.50e-03)	(3.72e-01)	(9.59e-03)	(3.10e-03)
	4	1.52e-01	1.59e-01	1.26e-01	3.53e-01	1.58e-01	1.53e-01	2.33e+00	1.33e-01	1.25e-01*
		(1.27e-03)	(7.46e-03)	(1.89e-03)	(3.88e-02)	(5.43e-03)	(9.04e-03)	(2.25e-01)	(4.64e-03)	(3.95e-03)
	8	1.70e-01	1.82e-01	1.45e-01*	3.67e-01	1.74e-01	1.86e-01	2.38e+00	1.62e-01	1.53e-01
		(7.76e-04)	(8.70e-03)	(3.17e-03)	(4.19e-02)	(4.81e-03)	(1.11e-02)	(3.15e-01)	(4.07e-03)	(3.33e-03)

Table 3: The average SMAPE of ESM-CNN and the counterparts.

Dataset	H	Training			Random			Ablation		Ours
		GS-CNN	DeepAR	CLSTM	RVFL	IELM	SCN	Stoc-CNN	ES-CNN	ESM-CNN
ARI	1	5.74e-02	5.81e-02	4.74e-02	3.02e+00	5.30e-02	3.40e-02	1.21e+00	2.33e-02	1.76e-02*
		(4.33e-03)	(1.28e-02)	(8.42e-03)	(6.74e+00)	(8.80e-03)	(1.35e-02)	(5.13e-01)	(5.13e-03)	(3.11e-04)
	3	6.73e-02	9.17e-02	6.61e-02	8.61e+00	5.76e-02	5.11e-02	1.50e+00	3.36e-02	2.72e-02*
		(4.23e-03)	(2.10e-02)	(8.15e-03)	(1.07e+01)	(7.44e-03)	(1.15e-02)	(1.36e+00)	(2.89e-03)	(1.04e-03)
	6	8.28e-02	1.25e-01	6.82e-02	6.36e+00	6.97e-02	6.28e-02	1.52e+00	4.78e-02	4.05e-02*
		(3.84e-03)	(2.41e-02)	(1.17e-02)	(6.59e+00)	(1.06e-02)	(1.62e-02)	(1.73e+00)	(3.03e-03)	(1.53e-03)
BTC	1	3.26e-02	1.29e-01	2.60e-01	5.04e+00	1.04e-01	5.93e-02	1.12e+00	2.37e-02	1.35e-02*
		(3.49e-03)	(2.02e-02)	(1.87e-02)	(7.64e+00)	(1.87e-02)	(1.44e-02)	(2.20e-01)	(9.73e-03)	(2.90e-04)
	3	3.35e-02	1.12e-01	2.87e-01	2.85e+00	1.04e-01	7.05e-02	1.09e+00	2.43e-02	1.48e-02*
		(3.65e-03)	(2.38e-02)	(1.97e-02)	(4.01e+00)	(1.85e-02)	(1.54e-02)	(1.26e-01)	(9.39e-03)	(2.10e-04)
	6	3.38e-02	1.36e-01	3.03e-01	2.69e+00	1.04e-01	7.68e-02	1.05e+00	2.48e-02	1.63e-02*
		(3.47e-03)	(2.76e-02)	(8.17e-03)	(4.68e+00)	(1.92e-02)	(1.52e-02)	(6.03e-02)	(8.99e-03)	(1.44e-04)
ILI	1	6.91e-02	6.02e-02	4.86e-02	1.28e-01	7.49e-02	6.06e-02	9.65e-01	5.20e-02	4.60e-02*
		(1.48e-03)	(4.37e-03)	(1.52e-03)	(1.73e-02)	(4.74e-03)	(5.13e-03)	(5.61e-01)	(5.09e-03)	(1.42e-03)
	4	8.40e-02	8.43e-02	6.71e-02	1.64e-01	8.83e-02	8.24e-02	1.39e+00	7.13e-02	6.65e-02*
		(7.92e-04)	(3.34e-03)	(1.09e-03)	(1.67e-02)	(3.64e-03)	(5.04e-03)	(4.77e-01)	(2.42e-03)	(1.97e-03)
	8	9.79e-02	1.00e-01	8.11e-02*	2.55e-01	1.01e-01	1.04e-01	1.60e+00	9.07e-02	8.52e-02
		(5.25e-04)	(3.68e-03)	(1.99e-03)	(1.63e-01)	(3.15e-03)	(6.38e-03)	(5.97e-01)	(2.25e-03)	(1.75e-03)

The results of comparison between ESM-CNN and the state-of-art competitors in Table 2, Table 3, and Table 4 lead to the following conclusions.

- 1) As the random neural network, ESM-CNN keeps promising accuracy and small variance

⁵<https://github.com/XinzeZhang/TimeSeriesForecasting-torch>

⁶<https://scikit-learn.org/stable/modules/preprocessing.html#preprocessing-scaler>

⁷<https://pytorch.org/>

Table 4: The average RMSE of ESM-CNN and the counterparts.

Dataset	H	Training			Random			Ablation		Ours
		GS-CNN	DeepAR	CLSTM	RVFL	IELM	SCN	Stoc-CNN	ES-CNN	ESM-CNN
AR1	1	5.53e-01 (3.60e-02)	5.08e-01 (9.60e-02)	4.89e-01 (8.93e-02)	3.21e+00 (1.85e+00)	5.54e-01 (7.81e-02)	3.34e-01 (1.13e-01)	4.36e+02 (2.01e+02)	2.28e-01 (3.43e-02)	1.55e-01* (3.66e-03)
	3	6.30e-01 (3.26e-02)	7.66e-01 (1.30e-01)	6.67e-01 (6.71e-02)	5.15e+00 (2.26e+00)	5.80e-01 (6.50e-02)	4.98e-01 (8.72e-02)	4.43e+02 (1.95e+02)	3.22e-01 (2.43e-02)	2.57e-01* (1.04e-02)
	6	7.40e-01 (2.55e-02)	9.96e-01 (1.34e-01)	6.79e-01 (9.10e-02)	5.59e+00 (3.27e+00)	6.71e-01 (7.89e-02)	6.00e-01 (1.27e-01)	1.07e+03 (5.37e+02)	4.61e-01 (2.71e-02)	3.94e-01* (1.62e-02)
BTC	1	3.87e+03 (3.62e+02)	1.15e+04 (1.52e+03)	2.08e+04 (1.15e+03)	6.74e+04 (3.63e+04)	1.05e+04 (1.60e+03)	6.52e+03 (1.41e+03)	1.33e+07 (1.11e+07)	2.75e+03 (1.07e+03)	1.59e+03* (2.39e+01)
	3	3.97e+03 (3.76e+02)	1.02e+04 (1.91e+03)	2.24e+04 (1.15e+03)	7.11e+04 (2.70e+04)	1.04e+04 (1.58e+03)	7.55e+03 (1.40e+03)	1.92e+07 (1.43e+07)	2.82e+03 (1.03e+03)	1.74e+03* (2.01e+01)
	6	4.00e+03 (3.54e+02)	1.22e+04 (2.12e+03)	2.33e+04 (4.55e+02)	8.82e+04 (3.93e+04)	1.04e+04 (1.64e+03)	8.09e+03 (1.33e+03)	2.30e+07 (1.96e+07)	2.89e+03 (9.79e+02)	1.92e+03* (1.51e+01)
ILI	1	8.45e-01 (1.95e-02)	7.82e-01 (1.87e-02)	7.10e-01 (2.52e-02)	1.74e+00 (3.17e-01)	8.88e-01 (4.41e-02)	7.14e-01 (3.11e-02)	1.50e+01 (2.50e+00)	6.81e-01 (5.37e-02)	6.06e-01* (8.14e-03)
	4	1.00e+00 (9.40e-03)	9.95e-01 (1.52e-02)	9.07e-01 (1.71e-02)	1.96e+00 (2.49e-01)	1.04e+00 (3.56e-02)	9.09e-01 (2.52e-02)	1.39e+01 (1.54e+00)	8.65e-01 (2.35e-02)	8.14e-01* (8.75e-03)
	8	1.16e+00 (5.03e-03)	1.16e+00 (2.11e-02)	1.04e+00 (1.76e-02)	2.00e+00 (2.32e-01)	1.18e+00 (2.07e-02)	1.11e+00 (2.54e-02)	1.43e+01 (2.03e+00)	1.07e+00 (1.07e-02)	1.03e+00* (6.63e-03)

on both artificial and real-world datasets, showing that ESM-CNN is robust and stable to practical applications.

- 2) In comparison with trained methods, GS-CNN outperforms DeepAR and CLSTM on the BTC dataset while CLSTM outperforms GS-CNN and DeepAR on the AR1 and ILI datasets, which shows that the convolutional architecture can be effectiveness for time series forecasting.
- 3) Compared with trained methods, taking the advantage of the convolutional architecture, ESM-CNN achieves the best RMSE on all datasets as well as all three prediction horizons and achieves almost the same percentage performance with CLSTM on ILI dataset, which demonstrates the effectiveness of ESM-CNN on characterizing the time series.
- 4) In comparison with random based counterparts, the incrementally constructed random MLPs (IELM and SCN) outperform the deterministic constructed RVFL, leading to the same conclusion in the related studies [16, 31] and showing the effectiveness of the incrementally constructive method.
- 5) Compared with random based counterparts, ESM-CNN also outperforms RVFL, IELM, and SCN on all datasets, showing the strong predictive power of ESM-CNN for time series forecasting.

The ablation study in Table 2, Table 3, and Table 4 shows the results as follows.

- 1) The Stoc-CNN, which uses purely deterministic random filters and the least square method to solve the output weights, achieves the worst performance on all tasks, indicating that the ill-posed problem occurs after globally configuring the output layer of the random CNN with a number of random filters.
- 2) The ES-CNN, which incrementally constructs the random convolutional layer and computes the output weights based on the error-feedback strategy, achieves a huge improvement of forecasting performance on Stoc-CNN, and shows the promising performance on all dataset, demonstrating the effectiveness of the incrementally constructive method for random CNN.

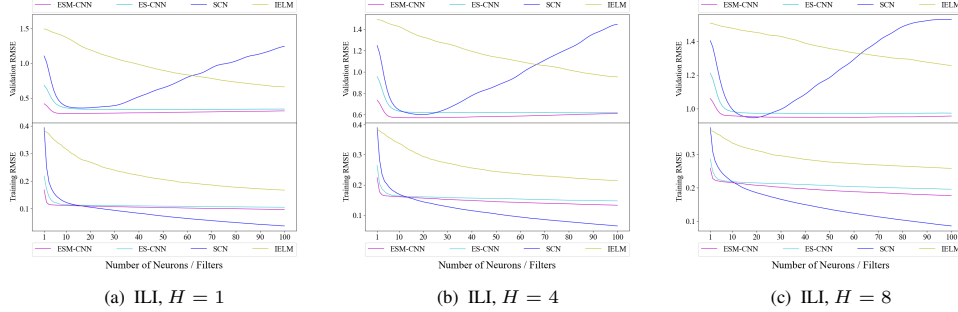


Figure 3: The average RMSE of incrementally constructed random neural networks on ILI dataset.

- 3) Based the comparison between ES-CNN and ESM-CNN, despite a narrow margin of the performance occurs on AR1 dataset, ESM-CNN surpasses ES-CNN in all experiments on real-world datasets (BTC and ILI), demonstrating the necessity of introducing the filter selection strategy to construct the random convolutional layer in ESM-CNN.

5.2. Comparison on Convergence

We further examine the convergence among the incrementally constructive modeling strategies (i.e., IELM, SCN, ES-CNN, and ESM-CNN). The averaged training and validation RMSE are plotted as the functions of the generated neurons or filters, which are shown in Figure 3. The results lead to the following conclusions.

- 1) Although we have examined various prediction horizons for each dataset, general conclusions are consistent with the different prediction horizons for all datasets.
- 2) Despite that SCN outperforms other models in terms of the rapid decreasing of RMSE on all training sets, it shows obvious overfitting on all validation sets. In contrast to SCN, IELM does not overfit on the training datasets but obviously converges slower than other models.
- 3) Via the error-feedback fully connected layer, ESM-CNN and ES-CNN outperform SCN and IELM on all validation sets, demonstrating the robustness and stability when considering the error-feedback strategy to construct random CNN for time series forecasting.
- 4) Comparing ESM-CNN with ES-CNN, despite that the convergence curves of the two strategies are close to each other, there are still remarkable findings. ESM-CNN steadily converges to a slightly but existentially lower RMSE on the training processes and exhibits better performance on the validation sets, which suggests the value of filter selection strategy.
- 5) For the convergence of the ESM-CNN and ES-CNN modeling strategies, the most significant improvements come from the early 10 constructive iterations. A possible explanation is that, the benefits from the error-feedback fully connected layer gradually vanishes as the number of filters increases, which gives a guidance that the smaller computation overheads may be enough to bring efficiency improvements on implementing ESM-CNN to time series prediction.

Here we try to provide an explanation to the overfitting issue of SCN and Stoc-CNN as well as the robustness of ESC-CNN and ES-CNN. The SCN and Stoc-CNN both globally compute

Table 5: The average running time (seconds) of each model on both two datasets.

Methods	Models	AR1			BTC			ILI		
		1	3	6	1	3	6	1	4	8
Training	GS-CNN	74.65	76.95	78.55	93.70	96.45	99.40	67.05	70.25	73.00
	DeepAR	225.25	238.95	257.70	223.75	251.10	268.65	256.80	279.10	275.30
	CLSTM	150.45	154.80	160.25	143.00	141.50	142.25	167.40	170.80	175.30
Random	RVFL	-	-	-	-	-	-	-	-	-
	IELM	2.65	2.85	2.80	3.40	3.30	3.20	2.55	2.55	2.40
	SCN	22.85	57.40	107.75	21.10	58.00	111.40	16.10	49.60	90.95
Ablation	Stoc-CNN	-	-	-	-	-	-	-	-	-
	ES-CNN	6.50	6.40	6.50	6.35	6.50	6.45	6.45	6.50	6.50
Our	ESM-CNN	9.65	9.65	9.70	7.10	7.25	7.25	7.15	7.15	7.20

all parameters of the fully connected output layer with the least square method, which makes the output parameters excessively complex and easily overfit on the noisy data of the training set. By contrast, the error-feedback modeling strategy of ESM-CNN and ES-CNN individually calculates the parameters of the newly added neuron at the error-feedback fully connected layer to compensate prediction error in the previous construction iteration. Thus, the influence of the noisy data is naturally reduced during the construction process, and the output weights are configured with a smaller norm than SCN and Stoc-CNN, enabling ESC-CNN and ES-CNN with higher robustness and stability.

Furthermore, the average running time (seconds) of each model on all datasets are shown in Table 5, The results show that, comparing with the trained models (GS-CNN, DeepAR, and CLSTM) as well as SCN, ESM-CNN and ES-CNN shows the competitive performance with a very short time. Besides, the proposed greedy based filter selection strategy in ESM-CNN only consumes a few additional time while bringing the significant improvements as shown in the subsection 5.1, demonstrating the efficiency of the ESM-CNN.

6. Conclusion

Time series forecasting is a challenging task due to the unsteady and dynamic innate property. In this work, we develop an error-feedback stochastic modeling strategy of convolutional neural network (ESM-CNN) for time series forecasting. Through the error-feedback stochastic modeling and the filter selection, ESM-CNN exhibits promising predictive power for time series forecasting with theoretical guarantee. The superiority of the proposed strategies with iteratively adding convolutional filters and configuring the corresponding error-feedback fully connected layer as well as the greedy based filter selection method are demonstrated experimentally.

In future work, we would like to try the ESM strategy to recurrent neural network architectures. Since the proposed ESM strategy widens the hidden layer with an incremental mechanism, we would also adapt this method to a hybrid architecture which consists of convolutional filters and recurrent cells in the same hidden layer, making the model benefit from the convolutional neural architectures and recurrent neural architectures simultaneously. Besides, we would propose a deep version of ESM strategy to utilize multiple layers to promote the forecasting performance.

7. Acknowledgment

This work was supported by Natural Science Foundation of China under Project Nos. 71571080 and 71871101, and Fundamental Research Fund for Central Universities under Project No.2019kfyXKJC021.

References

- [1] O. B. Sezer, A. M. Ozbayoglu, Algorithmic financial trading with deep convolutional neural networks: Time series to image conversion approach, *Applied Soft Computing* 70 (2018) 525–538.
- [2] S. Cavalli, M. Amoretti, CNN-based multivariate data analysis for bitcoin trend prediction, *Applied Soft Computing* 101 (2021) 107065.
- [3] Z. Luo, X. Cai, K. Tanaka, T. Takiguchi, T. Kinkyo, S. Hamori, Can we forecast daily oil futures prices? experimental evidence from convolutional neural networks, *Journal of risk and financial management* 12 (2019) 9.
- [4] N. Dong, J.-F. Chang, A.-G. Wu, Z.-K. Gao, A novel convolutional neural network framework based solar irradiance prediction method, *International Journal of Electrical Power & Energy Systems* 114 (2020) 105411.
- [5] H. J. Sadaei, P. C. d. L. e Silva, F. G. Guimarães, M. H. Lee, Short-term load forecasting by using a combined method of convolutional neural networks and fuzzy time series, *Energy* (2019).
- [6] P.-H. Kuo, C.-J. Huang, A high precision artificial neural networks model for short-term energy load forecasting, *Energies* 11 (2018) 213.
- [7] A. Zela, A. Klein, S. Falkner, F. Hutter, Towards automated deep learning: Efficient joint neural architecture and hyperparameter search, in: *International Conference on Machine Learning Workshop on AutoML*, 2018.
- [8] W. Hu, L. Yan, K. Liu, H. Wang, A short-term traffic flow forecasting method based on the hybrid PSO-SVR, *Neural Processing Letters* 43 (2016) 155–172.
- [9] J. J. Flores, M. Graff, H. Rodriguez, Evolutive design of ARMA and ANN models for time series forecasting, *Renewable Energy* 44 (2012) 225–230.
- [10] T. Elsken, J. H. Metzen, F. Hutter, Neural architecture search: A survey, *Journal of Machine Learning Research* 20 (2019) 1–21.
- [11] B. Baker, O. Gupta, R. Raskar, N. Naik, Accelerating neural architecture search using performance prediction, in: *International Conference on Learning Representations*, 2018.
- [12] K. He, Y. Wang, J. Hopcroft, A powerful generative model using random weights for the deep image representation, in: *Advances in Neural Information Processing Systems*, 2016, pp. 631–639.
- [13] J. M. Antognini, M. Hoffman, R. J. Weiss, Audio texture synthesis with random neural networks: Improving diversity and quality, in: *ICASSP 2019-2019 IEEE International Conference on Acoustics, Speech and Signal Processing (ICASSP)*, 2019, pp. 3587–3591.
- [14] W. Yu, M. Pacheco, Impact of random weights on nonlinear system identification using convolutional neural networks, *Information Sciences* 477 (2019) 1–14.
- [15] B. Igelnik, Y.-H. Pao, Stochastic choice of basis functions in adaptive function approximation and the functional-link net, *IEEE Transactions on Neural Networks* 6 (1995) 1320–1329.
- [16] D. Wang, M. Li, Stochastic configuration networks: Fundamentals and algorithms, *IEEE transactions on cybernetics* 47 (2017) 3466–3479.
- [17] H. Hewamalage, C. Bergmeir, K. Bandara, Recurrent neural networks for time series forecasting: Current status and future directions, *International Journal of Forecasting* 37 (2021) 388–427.
- [18] Y. LeCun, Y. Bengio, et al., Convolutional networks for images, speech, and time series, *The handbook of brain theory and neural networks* 3361 (1995) 1995.
- [19] Y. Bengio, A. Courville, P. Vincent, Representation learning: A review and new perspectives, *IEEE transactions on pattern analysis and machine intelligence* 35 (2013) 1798–1828.
- [20] B. Zhao, H. Lu, S. Chen, J. Liu, D. Wu, Convolutional neural networks for time series classification, *Journal of Systems Engineering and Electronics* 28 (2017) 162–169.
- [21] Y. Zheng, Q. Liu, E. Chen, Y. Ge, J. L. Zhao, Time series classification using multi-channels deep convolutional neural networks, in: *International Conference on Web-Age Information Management*, Springer, 2014, pp. 298–310.
- [22] J. Yang, M. N. Nguyen, P. P. San, X. L. Li, S. Krishnaswamy, Deep convolutional neural networks on multi-channel time series for human activity recognition, in: *Twenty-Fourth International Joint Conference on Artificial Intelligence*, 2015.
- [23] I. Koprinska, D. Wu, Z. Wang, Convolutional neural networks for energy time series forecasting, in: *2018 International Joint Conference on Neural Networks (IJCNN)*, 2018, pp. 1–8.
- [24] W. F. Schmidt, M. A. Kraaijveld, R. P. Duin, et al., Feed forward neural networks with random weights, in: *International Conference on Pattern Recognition*, IEEE COMPUTER SOCIETY PRESS, 1992, pp. 1–1.

- [25] G.-B. Huang, Q.-Y. Zhu, C.-K. Siew, Extreme learning machine: Theory and applications, *Neurocomputing* 70 (2006) 489–501.
- [26] Y.-H. Pao, G.-H. Park, D. J. Sobajic, Learning and generalization characteristics of the random vector functional-link net, *Neurocomputing* 6 (1994) 163–180.
- [27] S. Scardapane, D. Wang, M. Panella, A. Uncini, Distributed learning for Random Vector Functional-Link networks, *Information Sciences* 301 (2015) 271–284.
- [28] Y. Zhang, J. Wu, Z. Cai, B. Du, P. S. Yu, An unsupervised parameter learning model for RVFL neural network, *Neural Networks* 112 (2019) 85–97.
- [29] G.-B. Huang, H. Zhou, X. Ding, R. Zhang, Extreme Learning Machine for Regression and Multiclass Classification, *IEEE Transactions on Systems, Man, and Cybernetics, Part B (Cybernetics)* 42 (2012) 513–529.
- [30] L. L. C. Kasun, H. Zhou, G.-B. Huang, C. M. Vong, Representational learning with extreme learning machine for big data, *IEEE intelligent systems* 28 (2013) 31–34.
- [31] G.-B. Huang, L. Chen, C. K. Siew, et al., Universal approximation using incremental constructive feedforward networks with random hidden nodes, *IEEE Transactions on Neural Networks* 17 (2006) 879–892.
- [32] M. van Heeswijk, Y. Miche, T. Lindh-Knuutila, P. A. J. Hilbers, T. Honkela, E. Oja, A. Lendasse, Adaptive Ensemble Models of Extreme Learning Machines for Time Series Prediction, in: C. Alippi, M. Polycarpou, C. Panayiotou, G. Ellinas (Eds.), *Artificial Neural Networks – ICANN 2009, Lecture Notes in Computer Science*, Berlin, Heidelberg, 2009, pp. 305–314.
- [33] N. Zeng, H. Zhang, W. Liu, J. Liang, F. E. Alsaadi, A switching delayed PSO optimized extreme learning machine for short-term load forecasting, *Neurocomputing* 240 (2017) 175–182.
- [34] J. Wang, G. Athanasopoulos, R. J. Hyndman, S. Wang, Crude oil price forecasting based on internet concern using an extreme learning machine, *International Journal of Forecasting* 34 (2018) 665–677.
- [35] C. R. Vogel, *Computational methods for inverse problems*, volume 23, 2002.
- [36] M. Qi, G. P. Zhang, Trend time-series modeling and forecasting with neural networks, *IEEE Transactions on Neural Networks* 19 (2008) 808–816.
- [37] S. F. Crone, S. Häger, Feature selection of autoregressive neural network inputs for trend time series forecasting, in: *2016 International Joint Conference on Neural Networks (IJCNN)*, 2016, pp. 1515–1522.
- [38] G. Bontempi, Long term time series prediction with multi-input multi-output local learning, *Proc. 2nd ESTSP* (2008) 145–154.
- [39] D. Salinas, V. Flunkert, J. Gasthaus, T. Januschowski, DeepAR: Probabilistic forecasting with autoregressive recurrent networks, *International Journal of Forecasting* 36 (2020) 1181–1191.
- [40] I. E. Livieris, E. Pintelas, P. Pintelas, A CNN-LSTM model for gold price time-series forecasting, *Neural Computing and Applications* (2020) 1–10.
- [41] Y. Bao, T. Xiong, Z. Hu, Pso-mismo modeling strategy for multistep-ahead time series prediction, *IEEE transactions on cybernetics* 44 (2013) 655–668.
- [42] T. Guo, Z. Xu, X. Yao, H. Chen, K. Aberer, K. Funaya, Robust online time series prediction with recurrent neural networks, in: *2016 IEEE International Conference on Data Science and Advanced Analytics (DSAA)*, 2016, pp. 816–825.
- [43] Y. Zhao, J. Li, L. Yu, A deep learning ensemble approach for crude oil price forecasting, *Energy Economics* 66 (2017) 9–16.

Appendix A. Proof of the convergence of ESM-CNN

The intermediate prediction error sequence $\tilde{e}_{C+1}^0, \dots, \tilde{e}_{C+1}^{T-K+2}$ and intermediate parameters $\tilde{\beta}_{C+1}^0, \dots, \tilde{\beta}_{C+1}^{T-K+2}$ of the new added error-feedback fully connected layer are introduced as

$$\tilde{e}_{C+1}^{i+1} = \tilde{e}_{C+1}^i - \tilde{\beta}_{C+1}^{i+1} p_{C+1}^{i+1}, \quad i = 0, \dots, T - K + 1,$$

where

$$\begin{aligned} \tilde{\beta}_{C+1}^{i+1} &= [\tilde{\beta}_{C+1}^{i+1,1}, \dots, \tilde{\beta}_{C+1}^{i+1,h}, \dots, \tilde{\beta}_{C+1}^{i+1,H}], \\ \tilde{\beta}_{C+1}^{i+1,h} &= \langle \tilde{e}_{C+1}^{i+1}, p_{C+1}^{i+1} \rangle / \|p_{C+1}^{i+1}\|^2, \quad h = 1, \dots, H, \end{aligned}$$

and

$$\begin{aligned} \tilde{e}_{C+1}^0 &= e_C - \tilde{\beta}_{C+1}^0 p_{C+1}^0, \\ \tilde{\beta}_{C+1}^0 &= [\tilde{\beta}_{C+1}^{0,1}, \dots, \tilde{\beta}_{C+1}^{0,h}, \dots, \tilde{\beta}_{C+1}^{0,H}], \\ \tilde{\beta}_{C+1}^{0,h} &= \langle e_C^h, p_{C+1}^0 \rangle / \|p_{C+1}^0\|^2, \quad h = 1, \dots, H, \end{aligned}$$

making

$$\tilde{e}_{C+1}^{T-K+2} = e_C - \sum_{i=0}^{T-K+2} \tilde{\beta}_{C+1}^i p_{C+1}^i.$$

Since the parameters of the new added error-feedback fully connected layer are calculated by the least square method:

$$[\beta_{C+1}^0, \dots, \beta_{C+1}^{T-K+2}] = \underset{\beta}{\operatorname{argmin}} \|e_C - \sum_{i=0}^{T-K+2} \beta_{C+1}^i p_{C+1}^i\|,$$

the basic inequality between $\|e_{C+1}\|^2$ and $\|\tilde{e}_{C+1}^{T-K+2}\|^2$ holds:

$$\|e_{C+1}\|^2 = \min_{\beta} \|e_C - \sum_{i=0}^{T-K+2} \beta_{C+1}^i p_{C+1}^i\|^2 \leq \|e_C - \sum_{i=0}^{T-K+2} \tilde{\beta}_{C+1}^i p_{C+1}^i\|^2 = \|\tilde{e}_{C+1}^{T-K+2}\|^2.$$

Besides, the intermediate prediction error sequence is monotonically decreasing as:

$$\begin{aligned}
& \|\tilde{e}_{C+1}^{i+1}\|^2 - \|\tilde{e}_{C+1}^i\|^2 \\
&= \sum_{h=1}^H \left(\langle \tilde{e}_{C+1}^{i,h} - \tilde{\beta}_{C+1}^{i+1,h} p_{C+1}^{i+1}, \tilde{e}_{C+1}^{i,h} - \tilde{\beta}_{C+1}^{i+1,h} p_{C+1}^{i+1} \rangle - \langle \tilde{e}_{C+1}^{i,h}, \tilde{e}_{C+1}^{i,h} \rangle \right) \\
&= \sum_{h=1}^H \left(\langle \tilde{\beta}_{C+1}^{i+1} p_{C+1}^{i+1}, \tilde{\beta}_{C+1}^{i+1} p_{C+1}^{i+1} \rangle - 2 \langle \tilde{e}_{C+1}^{i,h}, \tilde{\beta}_{C+1}^{i+1} p_{C+1}^{i+1} \rangle \right) \\
&= \sum_{h=1}^H \left(\langle \frac{\langle \tilde{e}_{C+1}^{i,h}, p_{C+1}^{i+1} \rangle}{\|p_{C+1}^{i+1}\|^2} p_{C+1}^{i+1}, \frac{\langle \tilde{e}_{C+1}^{i,h}, p_{C+1}^{i+1} \rangle}{\|p_{C+1}^{i+1}\|^2} p_{C+1}^{i+1} \rangle - 2 \langle \tilde{e}_{C+1}^{i,h}, \frac{\langle \tilde{e}_{C+1}^{i,h}, p_{C+1}^{i+1} \rangle}{\|p_{C+1}^{i+1}\|^2} p_{C+1}^{i+1} \rangle \right) \\
&= \sum_{h=1}^H \left(\frac{\langle \tilde{e}_{C+1}^{i,h}, p_{C+1}^{i+1} \rangle^2}{\|p_{C+1}^{i+1}\|^4} \langle p_{C+1}^{i+1}, p_{C+1}^{i+1} \rangle - 2 \frac{\langle \tilde{e}_{C+1}^{i,h}, p_{C+1}^{i+1} \rangle}{\|p_{C+1}^{i+1}\|^2} \langle \tilde{e}_{C+1}^{i,h}, p_{C+1}^{i+1} \rangle \right) \\
&= \sum_{h=1}^H \left(\frac{\langle \tilde{e}_{C+1}^{i,h}, p_{C+1}^{i+1} \rangle^2}{\|p_{C+1}^{i+1}\|^4} \|p_{C+1}^{i+1}\|^2 - 2 \frac{\langle \tilde{e}_{C+1}^{i,h}, p_{C+1}^{i+1} \rangle^2}{\|p_{C+1}^{i+1}\|^2} \right) \\
&= \sum_{h=1}^H \left(- \langle \tilde{e}_{C+1}^{i,h}, p_{C+1}^{i+1} \rangle^2 / \|p_{C+1}^{i+1}\|^2 \right) \\
&\leq 0.
\end{aligned}$$

And the inequality between $\|\tilde{e}_{C+1}^0\|^2$ and $\|e_C\|^2$ can be proven by:

$$\begin{aligned}
& \|\tilde{e}_{C+1}^0\|^2 - \|e_C\|^2 \\
&= \sum_{h=1}^H \left(\langle e_C^h - \tilde{\beta}_{C+1}^{0,h} p_{C+1}^0, e_C^h - \tilde{\beta}_{C+1}^{0,h} p_{C+1}^0 \rangle - \langle e_C^h, e_C^h \rangle \right) \\
&= \sum_{h=1}^H \left(\langle \tilde{\beta}_{C+1}^{0,h} p_{C+1}^0, \tilde{\beta}_{C+1}^{0,h} p_{C+1}^0 \rangle - 2 \langle e_C^h, \tilde{\beta}_{C+1}^{0,h} p_{C+1}^0 \rangle \right) \\
&= \sum_{h=1}^H \left(\langle \frac{\langle e_C^h, p_{C+1}^0 \rangle}{\|p_{C+1}^0\|^2} p_{C+1}^0, \frac{\langle e_C^h, p_{C+1}^0 \rangle}{\|p_{C+1}^0\|^2} p_{C+1}^0 \rangle - 2 \langle e_C^h, \frac{\langle e_C^h, p_{C+1}^0 \rangle}{\|p_{C+1}^0\|^2} p_{C+1}^0 \rangle \right) \\
&= \sum_{h=1}^H \left(\frac{\langle e_C^h, p_{C+1}^0 \rangle^2}{\|p_{C+1}^0\|^4} \langle p_{C+1}^0, p_{C+1}^0 \rangle - 2 \frac{\langle e_C^h, p_{C+1}^0 \rangle}{\|p_{C+1}^0\|^2} \langle e_C^h, p_{C+1}^0 \rangle \right) \\
&= \sum_{h=1}^H \left(\frac{\langle e_C^h, p_{C+1}^0 \rangle^2}{\|p_{C+1}^0\|^4} \|p_{C+1}^0\|^2 - 2 \frac{\langle e_C^h, p_{C+1}^0 \rangle^2}{\|p_{C+1}^0\|^2} \right) \\
&= \sum_{h=1}^H \left(- \langle e_C^h, p_{C+1}^0 \rangle^2 / \|p_{C+1}^0\|^2 \right) \\
&\leq 0.
\end{aligned}$$

Then, the convergence of ESM-CNN can be proven by

$$\|e_{C+1}\|^2 \leq \|\tilde{e}_{C+1}^{T-K+2}\|^2 \leq \|\tilde{e}_{C+1}^0\|^2 \leq \|e_C\|^2.$$

Appendix B. Additional experiments

In this appendix, we consider eight more real-world datasets to evaluate our method to further strengthen the experiments. The additional datasets used in this study are as follows:

- *Weekly Europe Brent crude oil price* (BRENT-weekly),
- *Daily Europe Brent crude oil price* (BRENT-daily),
- *Weekly Cushing, OK WTI crude oil price* (WTI-weekly),
- *Daily Cushing, OK WTI crude oil price* (WTI-daily),
- *Daily close value of S&P 500 index* (S&P 500),
- *Daily close value of NASDAQ Composite* (NASDAQ),
- *Daily close value of Dow Jones Average* (DJI),
- *Daily close value of NYSE Composite* (NYSE).

Table B.6: The statistical information of the datasets.

Dataset	Stationarity	Trend	Seasonality	Period	Sample size
AR1	✗	0.97	0.09	-	500
BTC	✗	0.99	0.66	05/25/2020 ~ 11/23/2020	2181
ILI	✓	0.51	0.61	01/15/2010 ~ 04/15/2020	535
BRENT-weekly	✗	0.97	0.07	05/15/1987 ~ 04/30/2021	1773
BRENT-daily	✗	0.97	0.06	05/20/1987 ~ 05/03/2021	8620
WTI-weekly	✗	0.96	0.08	01/03/1986 ~ 04/30/2021	1844
WTI-daily	✗	0.96	0.07	01/02/1986 ~ 05/03/2021	8904
S&P 500	✗	0.99	0.40	12/31/2009 ~ 11/15/2017	1984
NASDAQ	✗	0.99	0.27	12/31/2009 ~ 11/15/2017	1984
DJI	✗	0.99	0.40	12/31/2009 ~ 11/15/2017	1984
NYSE	✗	0.98	0.45	12/31/2009 ~ 11/15/2017	1984

The Brent crude oil price datasets⁸ and WTI crude oil price datasets⁹ are respectively drawn from websites of the U.S. Energy Information Administration, And the other four financial datasets, i.e., S&P 500, NASDAQ, DJI, and NYSE, are collected from UCI Machine Learning Repository¹⁰. Table B.6 shows the statistical information of the additional datasets, where the stationarity was estimated with Augmented Dickey Fuller (ADF) test¹¹, the trend and seasonality are measured with its strength¹². For the column of stationarity, “✓” denotes the dataset is stationary, otherwise non-stationary. For the column of trend and seasonality, a bigger score represents a stronger strength of trend or seasonality.

As for the counterparts selection, we further consider three widely used statistical methods, i.e., naive forecasting (Naive), Autoregressive Integrated Moving Average (ARIMA), and Holt’s Winters Seasonal Exponential Smoothing (Holt), to validate our method. The embedding dimension T of weekly additional datasets, i.e., BRENT-weekly and WTI-weekly, are both set as 26 (half year), which are kept the same with weekly ILI dataset. The embedding dimension T of daily additional datasets, i.e., BRENT-daily, WTI-daily, S&P 500, NASDAQ, DJI, and NYSE, are set as 30 (six weeks).

The results of comparative experiments on all datasets are provided in Table B.7, Table B.8, and Table B.9 respectively, which lead to the same conclusion as in the main text.

⁸<https://www.eia.gov/dnav/pet/hist/RBRTed.htm>

⁹<https://www.eia.gov/dnav/pet/hist/rwtcW.htm>

¹⁰<https://archive.ics.uci.edu/ml/machine-learning-databases/00554/>

¹¹<https://www.statsmodels.org/stable/generated/statsmodels.tsa.stattools.adfuller.html>

¹²<https://otexts.com/fpp2/seasonal-strength.html>

Table B.7: The average MAPE of ESM-CNN and the counterparts.

Dataset	H	Statistical			Training			Random			Ablation		Ours
		Naive	ARIMA	Holt	CNN	DeepAR	CLSTM	RVFL	IELM	SCN	Stoc-CNN	ES-CNN	ESM-CNN
ARI	1	2.54e-01	5.95e-01	5.94e-01	1.06e-01	1.08e-01	8.88e-02	7.61e-01	9.84e-02	6.50e-02	6.10e+01	4.53e-02	3.49e-02*
	3	2.62e-01	6.00e-01	5.98e-01	1.23e-01	1.64e-01	1.20e-01	1.17e+00	1.07e-01	9.53e-02	6.34e+01	6.41e-02	5.28e-02*
	6	2.68e-01	6.08e-01	6.05e-01	1.48e-01	2.17e-01	1.24e-01	1.23e+00	1.26e-01	1.16e-01	1.54e+02	8.92e-02	7.70e-02*
BTC	1	2.55e-01	3.17e-01	3.17e-01	6.27e-02	2.26e-01	4.09e-01	1.20e+00	1.85e-01	1.11e-01	2.14e+02	4.62e-02	2.70e-02*
	3	2.54e-01	3.18e-01	3.18e-01	6.43e-02	1.98e-01	4.41e-01	1.13e+00	1.84e-01	1.29e-01	2.86e+02	4.73e-02	2.96e-02*
	6	2.53e-01	3.21e-01	3.20e-01	6.49e-02	2.35e-01	4.61e-01	1.38e+00	1.84e-01	1.40e-01	3.32e+02	4.84e-02	3.26e-02*
ILI	1	1.94e-01	5.70e-01	5.94e-01	1.28e-01	1.14e-01	9.50e-02	3.03e-01	1.38e-01	1.15e-01	2.48e+00	1.00e-01	8.93e-02*
	4	2.51e-01	5.39e-01	5.90e-01	1.52e-01	1.59e-01	1.26e-01	3.53e-01	1.58e-01	1.53e-01	2.33e+00	1.33e-01	1.25e-01*
	8	3.07e-01	5.34e-01	5.98e-01	1.70e-01	1.82e-01	1.45e-01*	3.67e-01	1.74e-01	1.86e-01	2.38e+00	1.62e-01	1.53e-01
BRENT-weekly	1	5.02e-01	1.09e-01	1.17e-01	1.60e-01	4.37e-02	8.25e-02	5.88e-02	1.57e-01	5.74e-02	1.93e+00	4.57e-02	3.97e-02*
	4	4.97e-01	2.13e-01	2.37e-01	1.78e-01	9.32e-02	1.15e-01	1.19e-01	1.73e-01	8.67e-02	2.87e+00	7.78e-02	7.49e-02*
	8	5.10e-01	3.26e-01	3.69e-01	1.82e-01	1.77e-01	1.85e-01	1.81e-01	2.12e-01	1.43e-01	3.70e+00	1.14e-01	1.11e-01*
BRENT-daily	1	4.80e-01	8.47e-02	8.92e-02	7.84e-02	1.93e-02*	3.51e-02	2.14e-02	1.36e-01	2.01e-02	5.06e-02	2.02e-02	1.99e-02
	5	4.82e-01	2.26e-01	2.45e-01	9.37e-02	3.48e-02	4.44e-02	3.92e-02	1.42e-01	3.50e-02	8.78e-02	3.42e-02	3.37e-02*
	10	4.88e-01	3.99e-01	4.34e-01	9.50e-02	5.18e-02	5.50e-02	5.51e-02	1.49e-01	5.10e-02	1.29e-01	5.37e-02	4.63e-02*
WTI-weekly	1	4.71e-01	9.99e-02	1.10e-01	2.26e-01	5.49e-02*	1.01e-01	7.10e-02	2.34e-01	6.33e-02	2.10e+00	6.27e-02	5.77e-02
	4	4.78e-01	2.06e-01	2.40e-01	2.47e-01	1.11e-01	1.45e-01	1.34e-01	2.53e-01	1.06e-01	3.11e+00	9.46e-02	8.64e-02*
	8	5.11e-01	3.18e-01	3.71e-01	2.46e-01	1.72e-01	2.16e-01	2.06e-01	2.81e-01	1.35e-01	3.70e+00	1.32e-01	1.24e-01*
WTI-daily	1	4.44e-01	7.82e-02	8.33e-02	9.30e-02	2.11e-02	3.62e-02	2.15e-02	1.45e-01	2.14e-02	7.24e-02	2.08e-02	2.06e-02*
	5	4.49e-01	2.05e-01	2.21e-01	9.90e-02	3.50e-02*	4.65e-02	4.14e-02	1.51e-01	3.67e-02	1.22e-01	3.62e-02	3.57e-02
	10	4.60e-01	3.57e-01	3.86e-01	9.96e-02	5.21e-02	5.76e-02	5.93e-02	1.58e-01	5.20e-02	1.67e-01	5.99e-02	4.99e-02*
S&P 500	1	1.50e-01	5.17e-03	8.26e-03	1.92e-02	1.28e-02	4.88e-02	8.82e-03	3.95e-02	1.18e-02	1.73e+00	5.33e-03	4.06e-03*
	5	1.46e-01	7.15e-03	1.10e-02	2.03e-02	1.87e-02	7.20e-02	1.91e-02	5.20e-02	2.20e-02	1.09e+01	7.03e-03	6.17e-03*
	10	1.48e-01	8.91e-03	1.32e-02	1.94e-02	7.97e-02	5.95e-02	2.40e-02	4.65e-02	3.46e-02	1.43e+01	8.71e-03	8.03e-03*
NASDAQ	1	1.77e-01	7.16e-03	1.04e-02	2.84e-02	7.19e-03	6.86e-02	3.65e-02	5.78e-02	1.62e-02	3.85e+01	6.68e-03	5.50e-03*
	5	1.73e-01	1.03e-02	1.40e-02	3.09e-02	2.15e-02	9.06e-02	3.50e-02	6.12e-02	2.36e-02	6.13e+01	9.12e-03	8.84e-03*
	10	1.75e-01	1.29e-02	1.73e-02	3.05e-02	1.53e-01	8.47e-02	3.52e-02	6.00e-02	4.35e-02	6.43e+01	1.15e-02	1.13e-02*
DJI	1	1.35e-01	5.24e-03	8.14e-03	2.36e-02	1.07e-02	4.28e-02	1.55e-02	4.73e-02	7.57e-03	6.20e+00	5.06e-03	4.09e-03*
	5	1.31e-01	7.53e-03	1.10e-02	2.54e-02	6.72e-02	6.54e-02	1.84e-02	4.72e-02	1.93e-02	4.73e+00	7.10e-03	6.71e-03*
	10	1.33e-01	9.55e-03	1.34e-02	2.56e-02	3.74e-02	6.64e-02	3.60e-02	4.70e-02	3.89e-02	7.16e+00	9.14e-03	9.06e-03*
NYSE	1	1.12e-01	5.61e-03	8.91e-03	1.31e-02	9.30e-03	1.53e-02	6.55e-03	2.63e-02	9.61e-03	6.68e-01	4.58e-03	4.52e-03*
	5	1.09e-01	7.68e-03	1.19e-02	1.44e-02	1.93e-02	2.30e-02	1.82e-02	2.65e-02	1.31e-02	9.32e-01	6.77e-03	6.69e-03*
	10	1.10e-01	9.24e-03	1.42e-02	1.53e-02	9.84e-02	2.89e-02	2.60e-02	2.69e-02	1.81e-02	1.45e+00	8.44e-03	8.38e-03*

Table B.8: The average SMAPE of ESM-CNN and the counterparts.

Dataset	H	Statistical			Training			Random			Ablation		Ours
		Naive	ARIMA	Holt	CNN	DeepAR	CLSTM	RVFL	IELM	SCN	Stoc-CNN	ES-CNN	ESM-CNN
ARI	1	1.33e-01	4.31e-01	4.30e-01	5.74e-02	5.81e-02	4.74e-02	3.02e+00	5.30e-02	3.40e-02	1.21e+00	2.33e-02	1.76e-02*
	3	1.37e-01	4.36e-01	4.34e-01	6.73e-02	9.17e-02	6.61e-02	8.61e+00	5.76e-02	5.11e-02	1.50e+00	3.36e-02	2.72e-02*
	6	1.46e-01	4.43e-01	4.40e-01	8.28e-02	1.25e-01	6.82e-02	6.36e+00	6.97e-02	6.28e-02	1.52e+00	4.78e-02	4.05e-02*
BTC	1	1.35e-01	1.90e-01	1.90e-01	3.26e-02	1.29e-01	2.60e-01	5.04e+00	1.04e-01	5.93e-02	1.12e+00	2.37e-02	1.35e-02*
	3	1.35e-01	1.91e-01	1.90e-01	3.35e-02	1.12e-01	2.87e-01	2.85e+00	1.04e-01	7.05e-02	1.09e+00	2.43e-02	1.48e-02*
	6	1.36e-01	1.93e-01	1.92e-01	3.38e-02	1.36e-01	3.03e-01	2.69e+00	1.04e-01	7.68e-02	1.05e+00	2.48e-02	1.63e-02*
ILI	1	9.82e-02	4.16e-01	4.47e-01	6.91e-02	6.02e-02	4.86e-02	1.28e-01	7.49e-02	6.06e-02	9.65e-01	5.20e-02	4.60e-02*
	4	1.22e-01	3.86e-01	4.44e-01	8.40e-02	8.43e-02	6.71e-02	1.64e-01	8.83e-02	8.24e-02	1.39e+00	7.13e-02	6.65e-02*
	8	1.55e-01	3.80e-01	4.54e-01	9.79e-02	1.00e-01	8.11e-02*	2.55e-01	1.01e-01	1.04e-01	1.60e+00	9.07e-02	8.52e-02
BRENT-weekly	1	3.25e-01	1.00e-01	9.90e-02	6.70e-02	2.07e-02	3.89e-02	2.82e-02	6.64e-02	2.84e-02	9.65e-01	2.26e-02	1.97e-02*
	4	9.68e-01	6.22e-01	3.17e-01	7.37e-02	4.17e-02	5.37e-02	5.42e-02	7.15e-02	4.19e-02	1.14e+00	3.79e-02	3.67e-02*
	8	3.68e-01	7.03e-01	4.40e-01	7.74e-02	7.57e-02	7.91e-02	8.30e-02	8.42e-02	6.06e-02	1.40e+00	5.35e-02	5.25e-02*
BRENT-daily	1	6.55e-01	1.63e-01	1.69e-01	3.67e-02	9.55e-03*	1.73e-02	1.05e-02	6.05e-02	9.92e-03	3.61e-02	1.00e-02	9.91e-03
	5	4.22e-01	5.21e-01	4.84e-01	4.31e-02	1.72e-02	2.18e-02	1.87e-02	6.26e-02	1.71e-02	6.66e-02	1.70e-02	1.67e-02*
	10	4.17e-01	7.59e-01	6.83e-01	4.38e-02	2.50e-02	2.68e-02	2.58e-02	6.51e-02	2.44e-02	1.39e-01	2.60e-02	2.28e-02*
WTI-weekly	1	3.69e-01	7.82e-02	9.42e-02	7.89e-02	2.06e-02*	4.17e-02	3.08e-02	8.89e-02	2.48e-02	6.86e-01	2.52e-02	2.44e-02*
	4	9.06e+01	2.10e-01	2.81e-01	8.50e-02	4.00e-02	5.86e-02	6.84e-02	9.40e-02	4.13e-02	8.43e-01	3.97e-02	3.90e-02*
	8	3.34e-01	3.80e-01	5.26e-01	8.43e-02	5.92e-02	7.93e-02	2.88e-01	1.00e-01	5.51e-02	2.75e+00	5.53e-02	5.17e-02*
WTI-daily	1	8.29e-01	1.34e-01	1.75e-01	4.26e-02	1.05e-02	1.78e-02	1.06e-02	6.45e-02	1.06e-02	1.17e-01	1.04e-02	1.02e-02*
	5	3.63e-01	6.75e-01	4.02e-01	4.50e-02	1.73e-02*	2.27e-02	1.95e-02	6.67e-02	1.79e-02	1.10e-01	1.76e-02	1.75e-02*
	10	4.20e-01	7.36e-01	8.09e-01	4.53e-02	2.51e-02	2.78e-02	2.73e-02	6.94e-02	2.47e-02	1.46e-01	2.83e-02	2.41e-02*
S&P 500	1	7.60e-02	2.59e-03	4.13e-03	9.68e-03	6.47e-03	2.53e-02	4.41e-03	2.03e-02	5.97e-03	5.23e+00	2.66e-03	2.03e-03*
	5	7.46e-02	3.58e-03	5.50e-03	1.02e-02	9.48e-03	3.79e-02	9.68e-03	2.69e-02	1.12e-02	4.37e+00	3.50e-03	3.08e-03*
	10	7.57e-02	4.47e-03	6.61e-03	9.81e-03	4.24e-02	3.11e-02	1.22e-02	2.40e-02	1.77e-02	7.42e+00	4.34e-03	4.02e-03*
NASDAQ	1	9.04e-02	3.58e-03	5.19e-03	1.44e-02	3.61e-03	3.61e-02	1.76e-02	3.00e-02	8.22e-03	1.34e+00	3.33e-03	2.75e-03*
	5	8.91e-02	5.15e-03	7.01e-03	1.57e-02	1.09e-02	4.85e-02	1.69e-02	3.19e-02	1.20e-02	1.88e+00	4.54e-03	4.42e-03*
	10	9.08e-02	6.50e-03	8.69e-03	1.55e-02	8.73e-02	4.53e-02	1.71e-02	3.12e-02	2.24e-02	1.77e+00	5.73e-03	5.66e-03*
DJI	1	6.83e-02	2.62e-03	4.08e-03	1.20e-02	5.36e-03	2.21e-02	7.66e-03	2.45e-02	3.80e-03	4.52e-01	2.52e-03	2.05e-03*
	5	6.71e-02	3.78e-03	5.51e-03	1.29e-02	3.58e-02	3.44e-02	9.04e-03	2.44e-02	9.78e-03	7.47e-01	3.54e-03	3.36e-03*
	10	6.81e-02	4.80e-03	6.74e-03	1.30e-02	1.92e-02	3.50e-02	1.73e-02	2.43e-02	2.01e-02	1.60e+00	4.57e-03	4.53e-03*
NYSE	1	5.63e-02	2.81e-03	4.46e-03	6.60e-03	4.67e-03	7.73e-03	3.28e-03	1.33e-02	4.83e-03	1.12e+00	2.29e-03	2.26e-03*
	5	5.52e-02	3.84e-03	5.98e-03	7.27e-03	9.77e-03	1.17e-02	9.21e-03	1.35e-02	6.59e-03	4.99e+00	3.38e-03	3.35e-03*
	10	5.61e-02	4.64e-03	7.12e-03	7.73e-03	5.49e-02	1.48e-02	1.33e-02	1.37e-02	9.13e-03	3.56e+00	4.22e-03	4.19e-03*

Table B.9: The average RMSE of ESM-CNN and the counterparts.

Dataset	H	Statistical			Training			Random			Ablation		Ours
		Naive	ARIMA	Holt	CNN	DeepAR	CLSTM	RVFL	IELM	SCN	Stoc-CNN	ES-CNN	ESM-CNN
ARI	1	1.16e+00	2.24e+00	2.23e+00	5.53e-01	5.08e-01	4.89e-01	3.21e+00	5.54e-01	3.34e-01	4.36e+02	2.28e-01	1.55e-01*
	3	1.19e+00	2.26e+00	2.25e+00	6.30e-01	7.66e-01	6.67e-01	5.15e+00	5.80e-01	4.98e-01	4.43e+02	3.22e-01	2.57e-01*
	6	1.25e+00	2.29e+00	2.28e+00	7.40e-01	9.96e-01	6.79e-01	5.59e+00	6.71e-01	6.00e-01	1.07e+03	4.61e-01	3.94e-01*
BTC	1	1.47e+04	1.49e+04	1.49e+04	3.87e+03	1.15e+04	2.08e+04	6.74e+04	1.05e+04	6.52e+03	1.33e+07	2.75e+03	1.59e+03*
	3	1.47e+04	1.49e+04	1.49e+04	3.97e+03	1.02e+04	2.24e+04	7.11e+04	1.04e+04	7.55e+03	1.92e+07	2.82e+03	1.74e+03*
	6	1.46e+04	1.50e+04	1.50e+04	4.00e+03	1.22e+04	2.33e+04	8.82e+04	1.04e+04	8.09e+03	2.30e+07	2.89e+03	1.92e+03*
ILI	1	9.44e-01	2.23e+00	2.28e+00	8.45e-01	7.82e-01	7.10e-01	1.74e+00	8.88e-01	7.14e-01	1.50e+01	6.81e-01	6.06e-01*
	4	1.28e+00	2.25e+00	2.35e+00	1.00e+00	9.95e-01	9.07e-01	1.96e+00	1.04e+00	9.09e-01	1.39e+01	8.65e-01	8.14e-01*
	8	1.63e+00	2.36e+00	2.47e+00	1.16e+00	1.16e+00	1.04e+00	2.00e+00	1.18e+00	1.11e+00	1.43e+01	1.07e+00	1.03e+00*
BRENT-weekly	1	3.24e+01	7.23e+00	7.49e+00	1.01e+01	2.90e+00	5.21e+00	3.86e+00	9.91e+00	3.73e+00	2.67e+02	2.89e+00	2.62e+00*
	4	3.21e+01	1.70e+01	1.78e+01	1.12e+01	6.06e+00	7.75e+00	9.06e+00	1.08e+01	5.81e+00	3.83e+02	5.20e+00	5.14e+00*
	8	3.31e+01	2.96e+01	3.13e+01	1.12e+01	1.15e+01	1.13e+01	1.41e+01	1.31e+01	9.31e+00	4.86e+02	7.61e+00	7.52e+00*
BRENT-daily	1	3.14e+01	5.89e+00	5.95e+00	5.22e+00	1.32e+00*	2.29e+00	1.44e+00	8.70e+00	1.35e+00	4.19e+00	1.35e+00	1.34e+00
	5	3.17e+01	1.88e+01	1.88e+01	6.19e+00	2.34e+00	2.93e+00	2.70e+00	9.05e+00	2.35e+00	7.92e+00	2.32e+00	2.29e+00*
	10	3.21e+01	3.53e+01	3.51e+01	6.26e+00	3.82e+00	3.73e+00	3.75e+00	9.48e+00	3.41e+00	1.19e+01	3.68e+00	3.16e+00*
WTI-weekly	1	2.87e+01	7.00e+00	7.31e+00	1.22e+01	2.64e+00*	5.35e+00	4.04e+00	1.24e+01	3.08e+00	2.36e+02	3.05e+00	2.81e+00*
	4	2.91e+01	1.60e+01	1.68e+01	1.34e+01	5.92e+00	8.39e+00	9.19e+00	1.33e+01	5.50e+00	3.65e+02	5.21e+00	5.01e+00*
	8	2.95e+01	2.79e+01	2.94e+01	1.34e+01	8.93e+00	1.43e+01	1.42e+01	1.45e+01	7.51e+00	4.25e+02	7.65e+00	7.21e+00*
WTI-daily	1	2.83e+01	5.37e+00	5.43e+00	5.97e+00	1.37e+00	2.24e+00	1.39e+00	8.91e+00	1.41e+00	6.97e+00	1.37e+00	1.35e+00*
	5	2.85e+01	1.71e+01	1.69e+01	6.36e+00	2.24e+00*	2.92e+00	2.79e+00	9.26e+00	2.41e+00	1.25e+01	2.33e+00	2.32e+00*
	10	2.89e+01	3.23e+01	3.15e+01	6.43e+00	3.54e+00	3.85e+00	4.08e+00	9.70e+00	3.39e+00	1.74e+01	3.84e+00	3.23e+00*
S&P 500	1	4.24e+02	1.67e+01	2.49e+01	5.48e+01	3.46e+01	1.47e+02	2.61e+01	1.15e+02	3.44e+01	5.89e+03	1.56e+01	1.28e+01*
	5	4.20e+02	2.22e+01	3.32e+01	5.77e+01	5.29e+01	2.09e+02	5.58e+01	1.45e+02	6.34e+01	4.22e+04	2.12e+01	1.93e+01*
	10	4.23e+02	2.75e+01	4.00e+01	5.49e+01	2.39e+02	1.71e+02	6.83e+01	1.34e+02	1.01e+02	5.56e+04	2.58e+01	2.43e+01*
NASDAQ	1	1.23e+03	5.42e+01	7.54e+01	2.07e+02	4.99e+01	5.17e+02	3.20e+02	4.30e+02	1.29e+02	3.70e+05	4.95e+01	4.24e+01*
	5	1.22e+03	7.41e+01	1.02e+02	2.23e+02	1.57e+02	6.80e+02	3.44e+02	4.51e+02	1.79e+02	5.97e+05	6.75e+01	6.54e+01*
	10	1.23e+03	9.38e+01	1.26e+02	2.18e+02	1.19e+03	6.56e+02	3.19e+02	4.41e+02	3.16e+02	6.22e+05	8.36e+01	8.29e+01*
DJI	1	3.32e+03	1.44e+02	2.09e+02	6.28e+02	2.70e+02	1.19e+03	4.56e+02	1.26e+03	2.06e+02	2.64e+05	1.30e+02	1.10e+02*
	5	3.29e+03	2.03e+02	2.87e+02	6.72e+02	1.98e+03	1.76e+03	6.17e+02	1.25e+03	5.07e+02	2.02e+05	1.84e+02	1.80e+02*
	10	3.32e+03	2.59e+02	3.58e+02	6.70e+02	1.01e+03	1.80e+03	1.27e+03	1.23e+03	1.07e+03	2.85e+05	2.36e+02	2.33e+02*
NYSE	1	1.55e+03	8.98e+01	1.33e+02	1.84e+02	1.27e+02	2.31e+02	9.40e+01	3.64e+02	1.42e+02	1.66e+04	6.97e+01	6.86e+01*
	5	1.54e+03	1.17e+02	1.76e+02	2.02e+02	2.90e+02	3.45e+02	2.82e+02	3.68e+02	1.93e+02	2.28e+04	1.05e+02	1.03e+02*
	10	1.55e+03	1.38e+02	2.10e+02	2.14e+02	1.68e+03	4.31e+02	4.05e+02	3.72e+02	2.56e+02	3.93e+04	1.28e+02	1.26e+02*